Title

New constraints on equatorial temperatures during a Late Neoproterozoic snowball Earth glaciation

Authors

Ewing, Ryan C
Eisenman, Ian
Lamb, Michael P
et al.

Publication Date

2014-11-01

DOI

10.1016/j.epsl.2014.09.017

Peer reviewed

Earth and Planetary Science Letters 406 (2014) 110–122

Contents lists available at ScienceDirect

Earth and Planetary Science Letters

www.elsevier.com/locate/epsl

New constraints on equatorial temperatures during a Late Neoproterozoic snowball Earth glaciation

Ryan C. Ewing [a,*], Ian Eisenman [b], Michael P. Lamb [c], Laura Poppick [d], Adam C. Maloof [d], Woodward W. Fischer [c]

[a] Department of Geology and Geophysics, Texas A&M University, College Station, TX 77843, United States
[b] Scripps Institution of Oceanography, University of California at San Diego, La Jolla, CA 92093, United States
[c] Division of Geological and Planetary Sciences, California Institute of Technology, Pasadena, CA 91125, United States
[d] Department of Geosciences, Princeton University, Princeton, NJ 08544, United States

ARTICLE INFO

Article history:
Received 10 April 2014
Received in revised form 27 August 2014
Accepted 9 September 2014
Available online 28 September 2014
Editor: J. Lynch-Stieglitz

Keywords:
paleoclimate
Cryogenian
aeolian
periglacial
snowball Earth

ABSTRACT

Intense glaciation during the end of Cryogenian time (~635 million years ago) marks the coldest climate state in Earth history – a time when glacial deposits accumulated at low, tropical paleolatitudes. The leading idea to explain these deposits, the snowball Earth hypothesis, predicts globally frozen surface conditions and subfreezing temperatures, with global climate models placing surface temperatures in the tropics between −20 °C and −60 °C. However, precise paleosurface temperatures based upon geologic constraints have remained elusive and the global severity of the glaciation undetermined. Here we make new geologic observations of tropical periglacial, aeolian and fluvial sedimentary structures formed during the end-Cryogenian, Marinoan glaciation in South Australia; these observations allow us to constrain ancient surface temperatures. We find periglacial sand wedges and associated deformation suggest that ground temperatures were sufficiently warm to allow for ductile deformation of a sandy regolith. The wide range of deformation structures likely indicate the presence of a paleoactive layer that penetrated 2–4 m below the ground surface. These observations, paired with a model of ground temperature forced by solar insolation, constrain the local mean annual surface temperature to within a few degrees of freezing. This temperature constraint matches well with our observations of fluvial deposits, which require temperatures sufficiently warm for surface runoff. Although this estimate coincides with one of the coldest near sea-level tropical temperatures in Earth history, if these structures represent peak Marinaon glacial conditions, they do not support the persistent deep freeze of the snowball Earth hypothesis. Rather, surface temperatures near 0 °C allow for regions of seasonal surface melting, atmosphere–ocean coupling and possible tropical refugia for early metazoans. If instead these structures formed during glacial onset or deglaciation, then they have implications for the timescale and character for the transition into or out of a snowball state.

1. Introduction

Observations of globally-distributed glacial sediments deposited at sea-level in low paleolatitudes (Harland, 2007; Hoffman and Schrag, 2002; Williams, 1975) gave rise to claims that Earth's late Neoproterozoic glacial climate must have been radically different from that of Phanerozoic glacial intervals (Hoffman and Schrag, 2002; Hoffman et al., 1998; Kirschvink, 1992; Williams, 1975). The origin and significance of these glaciogenic deposits has been debated for nearly a century (see review in Harland, 2007), but the snowball Earth hypothesis has emerged as a unifying hypothesis to explain the evidence. The snowball Earth model proposes that Cryogenian climatic events drove equatorial temperatures to below −20 °C, temperatures sufficient to freeze Earth's oceans from pole to equator (Hoffman and Schrag, 2002; Kirschvink, 1992). Variants on the snowball Earth model propose that the equatorial regions of Earth's oceans remained open and Earth's surface temperatures, though cold, were not sufficient to freeze the entirety of Earth's surface (Abbot et al., 2011; Crowley et al., 2001; Peltier et al., 2007). Direct geological constraints on surface temperatures during this period are missing, and evidence supporting any one hypothesis has thus far been equivocal.

Although abundant glacial sediments deposited at low latitudes during Cryogenian time provide the primary evidence for a cold

* Corresponding author.
E-mail address: rce@geos.tamu.edu (R.C. Ewing).

http://dx.doi.org/10.1016/j.epsl.2014.09.017
0012-821X/

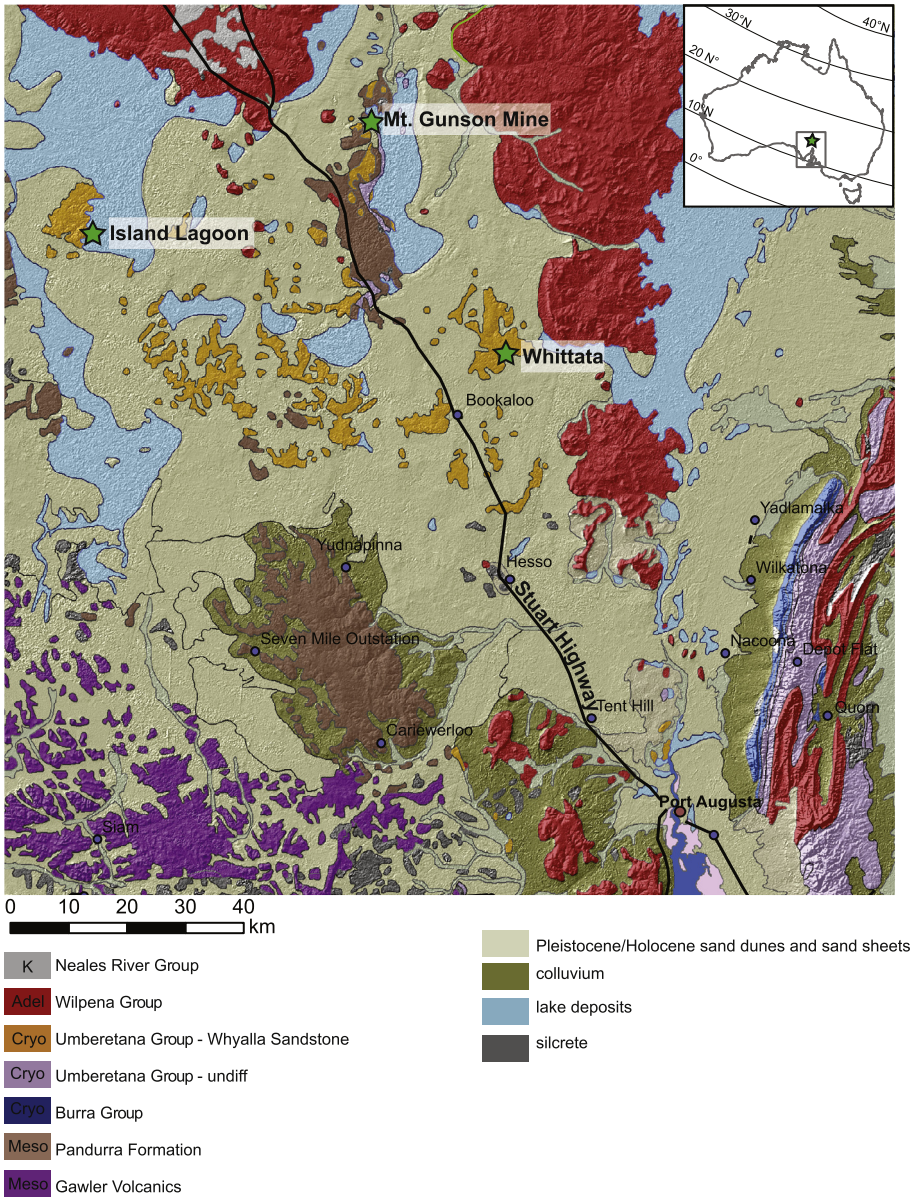

Fig. 1. Generalized geological map of the Stuart Shelf and Adelaide Rift Complex in South Australia. Outcrop localities are labeled. Inset map shows paleolatitude of Australia (Evans and Raub, 2011; Schmidt et al., 2009; Sohl et al., 1999; Sumner et al., 1987).

global climate, significant differences in the environment are expected depending on the temperature of Earth's surface. For example, at the temperatures expected by the end-member model of a snowball Earth, the range of active sedimentary processes during the peak glacial periods would be limited (Allen and Etienne, 2008). Wind-blown sediments may be made unavailable for transport because of ice burial or ice cementation. Temperatures would be too cold for fluvial activity and modification of continental shelf sediments by tidal and wave action would be greatly attenuated (Hoffman and Schrag, 2002). Models that do not require deeply frozen temperatures allow a wider range of sedimentary environments associated with an active hydrologic cycle and open oceans to be active throughout the glaciation and, in certain localities, such sedimentary environments have been highlighted as counter evidence to the presence of a snowball Earth during the Cryogenian (Allen and Etienne, 2008).

Periglacial sand wedges and associated regolith deformation and fluvial deposits found in the Marinoan Whyalla Sandstone in South Australia, are a primary focus of this study (Fig. 1). This suite of sedimentary structures forms under a relatively narrow thermal regime (Mellon, 1997; Pewe, 1959) and can be used to refine equatorial temperature estimates during the Marinoan glaciation. Models and modern observations of sand wedges indicate that wedges form by sediment infilling of thermal contraction cracks, which occur when the ground cools and induces a tensile stress that exceeds the strength of frozen regolith (Maloof et al., 2002; Mellon, 1997; Pewe, 1959). Large seasonal temperature variations found at high latitudes, very cold ground (mean annual temperature $< 0\,^{\circ}C$), and a dry climate are key characteristics of these models and observations that indicate crack and fill cycles that give rise to vertically laminated, sand-filled wedges, which may be associated with deformed ground (Fig. 2) (Black, 1976; Hallet et al., 2011; Pewe, 1959; Sletten et al., 2003). Deformed ground associated with sand wedge growth occurs because sand fills the open fracture and during a warm phase of the cycle the ground expands; the fracture cannot close and compressive stresses propagate horizontally to deform the ground surrounding the wedge (Hallet et al., 2011).

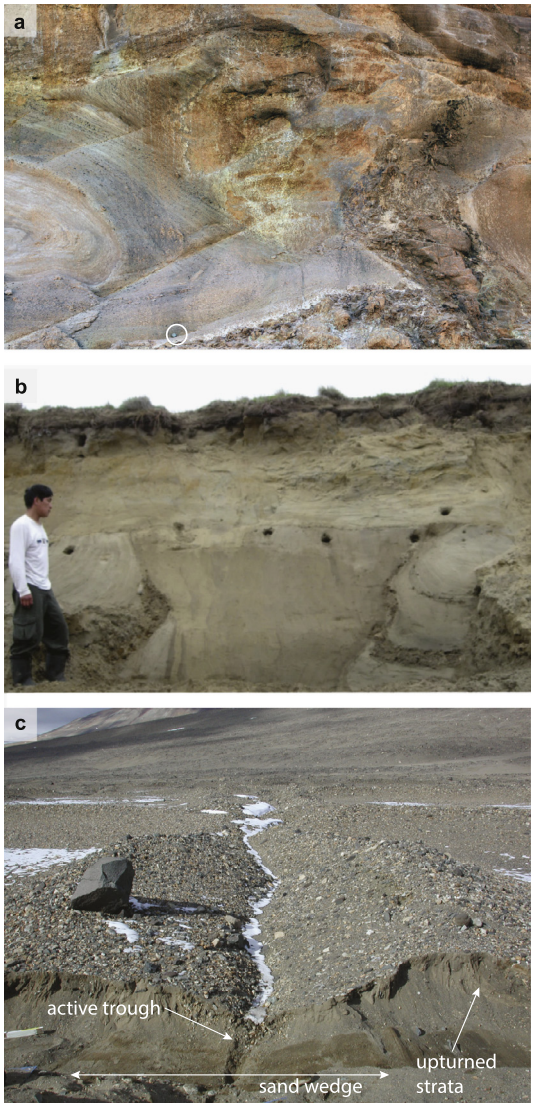

Fig. 2. Images of sand wedges from different times and localities. Sand wedge formed in Marinoan-age aeolian Whyalla Sandstone, South Australia (a), Pleistocene sand-sheet deposits in Arctic Canada (Murton and Bateman, 2007) (photo courtesy J. Murton) and (c) Holocene deposits in Antarctica (photo courtesy R. Sletten). Upturned, convolute bedding is present in each image adjacent to the sand wedge. Sand wedge in (c) is shown in cross-section and plan view and shows relief generated from the wedge expansion. This relief has been eroded and buried in the (a) and (b). White circle encompasses a coin for scale in (a) and a 20 cm ruler is visible on the left side of the image in (c).

Some of these structures have long presented a conundrum for reconstructing Earth's equatorial climate during the Marinoan glaciation in South Australia. The presence of sand wedges in particular, because they are thought to require a strong seasonal temperature variation, are difficult to explain at equatorial latitudes where seasonal temperature variations are low. Their presence in the low latitudes, along with low-latitude glacial deposits, inspired the proposal that Earth's obliquity was higher prior to the Cambrian Period (Williams, 1975, 2007). An alternative hypothesis suggested that the wedges formed by diurnal temperature variations under severely cold equatorial conditions, consistent with the snowball Earth hypothesis (Maloof et al., 2002).

Here we revisit the origin of these sand wedges in the context of other co-existing sedimentary structures and paleoenvironments. In order to explain these features and place constraints on the paleotemperatures during the Marinoan Glaciation in South Australia, we pair geologic observations with a model of ground temperatures forced by solar insolation. The model provides a better understanding of the expected temperature change within which low-paleolatitude sedimentary deposits develop, and it is used along with observations of periglacial sand wedges to constrain temperatures. Observations of an active fluvial system corroborate the primary conclusion of this work that temperatures during the Marinoan glaciation in South Australia were warmer than anticipated by a snowball Earth and were likely near 0 °C.

2. Geologic background

The Cryogenian Whyalla Sandstone and Cattle Grid Breccia contain abundant sand wedges, periglacial deformation structures, and aeolian and fluvial deposits. These deposits sit on the Stuart Shelf, which is adjacent to the Adelaide Rift Complex (ARC) (Preiss, 1987; Williams and Tonkin, 1985; Williams, 1998). During Late Neoproterozoic time, the Stuart Shelf and ARC were part of a broad continental margin undergoing episodes of rifting and thermal subsidence, which provided accommodation for a 7–12 km succession of Neoproterozoic to Cambrian deposits, directly overlying Paleo- and Mesoproterozoic basement (Preiss, 1987). The relatively undeformed Stuart Shelf lies to the west of the ARC and preserves thin, Neoproterozoic to Cambrian cratonic cover that onlaps the Gawler Craton (Fig. 1).

2.1. Stratigraphy

The Whyalla Sandstone is part of the Umberatana Group, which is the primary Cryogenian glaciogenic sedimentary succession in South Australia. The Whyalla Sandstone is interpreted as a periglacial aeolian sand sheet and thought to correlate down stratigraphic dip to the laminated siltstones and tillites of the syn-Marinoan, glacio-marine Elatina Formation (Preiss, 1987). Outcrop exposure between the Stuart Shelf and the ARC is poor and the correlation is primarily based upon the cold-climate facies association between the glacial Elatina Formation and periglacial Whyalla Sandstone (Preiss, 1987; Williams et al., 2008). The correlation between the Whyalla Sandstone and the Elatina Formation is strengthened by subsurface cores that demonstrate that the Nuccaleena Formation cap carbonate, which overlies the Elatina Formation, also overlies the Whyalla Sandstone in the subsurface (McGlown et al., 2012; Williams, 1998). The Nuccaleena Formation is part of the younger Wilpena Group: the base of the formation is associated with post-glacial transgression and marks the beginning of the Ediacaran Period (Preiss, 1987; Rose and Maloof, 2010). The Nuccaleena has been correlated globally by distinctive lithofacies and chemostratigraphic analysis to other Marinoan-age cap carbonates (Hoffman, 2011).

Our analysis focuses on periglacial structures located at and near the Mt. Gunson Mine on the Stuart Shelf (Fig. 1). This area of the Stuart Shelf is thought to have been a paleo-high, denoted as the Pernatty Upwarp, during deposition of the Whyalla Sandstone and generation of the periglacial structures (Preiss, 1987; Williams and Tonkin, 1985; Williams, 1998). At the mine, the underlying basement is the Mesoproterozoic Pandurra Formation, which consists of very coarse fluvial sandstone and pebble conglomerates. The upper Pandurra Formation at the mine is highly brecciated and known as the Cattle Grid Breccia (Williams and Tonkin, 1985). The breccia is thought to represent long-term exposure to cryogenic processes during the Cryogenian period (Williams and Tonkin, 1985), and it does not appear in outcrops or drill cores elsewhere on the Stuart Shelf away from the Pernatty Upwarp.

2.2. Age and paleogeography

Paleomagnetic constraints have not been determined directly from the Whyalla Sandstone, but constraints from the Elatina

Formation and overlying Nuccaleena Formation place the ARC at < 15° North paleolatitude, with best current estimates between 7° and 14° North paleolatitude (Evans and Raub, 2011; Hoffman and Li, 2009; Schmidt et al., 2009; Sohl et al., 1999; Sumner et al., 1987). The precise paleogeographic location of the Elatina Formation is a subject of some debate based upon the stratigraphic relationship between the Elatina Formation, which is estimated at 10° North (Schmidt et al., 2009), and the overlying Nuccaleena Formation which is estimated at 14° North (Evans and Raub, 2011). Preiss (2000) and Williams et al. (2008) report a basin-wide sequence boundary at the contact between the formations. However, Rose and Maloof (2010) conclude that no regional unconformity exists between the Elatina Formation and Nuccaleena Formation based upon forty-one measured stratigraphic sections from outcrop across the ARC. In their study, no angular relationship was observed that indicated an unconformity, the thickness of the Nuccaleena Formation was largely constant across the Flinders Ranges, and the contact varied from sharp and winnowed to transitional with silt and ice-rafted debris. Despite a debate over the precise location, all studies place the Elatina Formation and hence the correlative Whyalla Sandstone at less than 15° North paleolatitude (Evans and Raub, 2011; Hoffman and Li, 2009; Schmidt et al., 2009).

Although absolute age constraints for the Whyalla Sandstone remain elusive, the minimum age is reasonably well constrained by regional correlation to the Elatina Formation and by global chemo and litho stratigraphic correlation of the Nuccaleena cap carbonate (Hoffman, 2011). The Whyalla Sandstone is thought to have been deposited during the Marinoan glaciation prior to 635 Ma; this date is constrained by radiometric ages associated with cap carbonates in Namibia and China (Bowring et al., 2007; Condon et al., 2005; Hoffmann et al., 2004). Recent detrital zircon (DZ) analysis by Rose et al. (2013) demonstrates that the youngest DZ ages within the Elatina Formation approach 635 Ma, consistent with the Elatina Formation being a syn-Marinoan glacial deposit, whereas the youngest DZ ages from the Whyalla Sandstone cluster near 680 Ma. In addition to the difference in the youngest ages, the DZ age spectra between the Elatina Formation and the Whyalla Sandstone are different. The Whyalla Sandstone shows a distinct peak that matches that of the Pandurra Formation, suggesting the Pandurra is a primary source for the Whyalla Sandstone sediments. The Elatina Formation has no such peak and overall different age spectra from that of the Whyalla Sandstone. Given the stratigraphic constraint of the overlying Nuccaleena Formation that ties the Elatina Formation and Whyalla Sandstone, the origin of the difference in the youngest ages and the provenance between the Whyalla Sandstone and the Elatina Formation remains unclear, although some evidence points to a difference in sediment provenance.

3. Periglacial, aeolian, and fluvial sedimentology

3.1. Mt. Gunson Mine, South Australia

Our primary observations of aeolian stratigraphy, sand wedges, and periglacial deformation structures were made from the NW and NE pits of the Mt. Gunson Mine, South Australia, which are separated by less than 1 km. Sand wedges and deformation structures at this locality are developed on the Cattle Grid Breccia and within overlying aeolian sand sheet and dune strata of the Whyalla Sandstone (Fig. 3). Within the NW pit, the Whyalla Sandstone consists of three well-exposed sedimentary facies (Fig. 4a). The lowermost facies consists of large sand wedges, contorted bedding, diapirs, and periglacial involutions developed within a medium- to coarse-grained sandstone with matrix-supported clasts of the underlying, brecciated Pandurra Formation ranging up to 50 cm. Sand wedges range up to 3.5 m in width and 2.5 m deep within

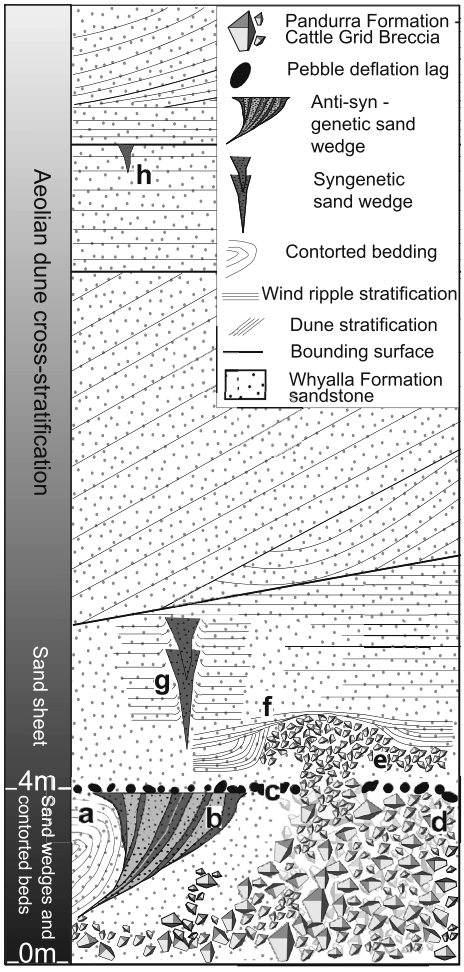

Fig. 3. Composite stratigraphic column of the Whyalla Sandstone and Cattle Grid Breccia at the Mt. Gunson Mine. (a) Contorted bedding in Whyalla Sandstone. (b) Anti-syngenetic sand wedge. (c) Pebble lag surface. (d) Cattle Grid Breccia. (e) Diapiric structure. (f) Onlapping relationship of sand sheet facies with diapiric structure. (g) Syngenetic genetic sand wedges. (h) Sand wedge within aeolian dune cross-stratification.

the Cattle Grid Breccia in the NW and NE Pits (Fig. 4, b, c and d). This facies is overlain by a medium- to coarse-grained sandstone with minor sand wedges and wind ripple lamination, which is interpreted as a periglacial aeolian sand sheet (Williams, 1998). Sets of aeolian cross-stratification ranging up to 12 m thick with rare minor sand wedges sit above the wind rippled facies and form the bulk of the Whyalla Sandstone at this locality (Figs. 3 and 4). Dry accumulation of the aeolian strata is indicated by the absence of damp or wet interdune flat strata as primary set bounding surfaces, which is characterized by wavy lamination, soft-sediment deformation, biotic crusts and evaporites (Kocurek and Havholm, 1993). Within the NE Pit, the Cattle Grid Breccia with sand wedges and convolute bedding comprises the lower-most facies. Aeolian sand sheets with minor sand wedges overly the breccia and large sets of aeolian cross-strata sit above the sand sheet (Fig. 3 and Fig. 4, b and c). At several locations within the NE pit, the deformation of the Cattle Grid Breccia gives way downward to undeformed Pandurra Formation sandstone, with only minor brecciation.

The largest wedges in both locations terminate upward into a deflation surface with pebble lag (Fig. 3), suggesting that these wedges were either epigenetic, having persisted for an extended period on a stable surface, or anti-syngenetic, with the wedges forming during deflation of the surface (Mackay, 1990; Murton and Bateman, 2007). Sand sheet laminations onlap relict topog-

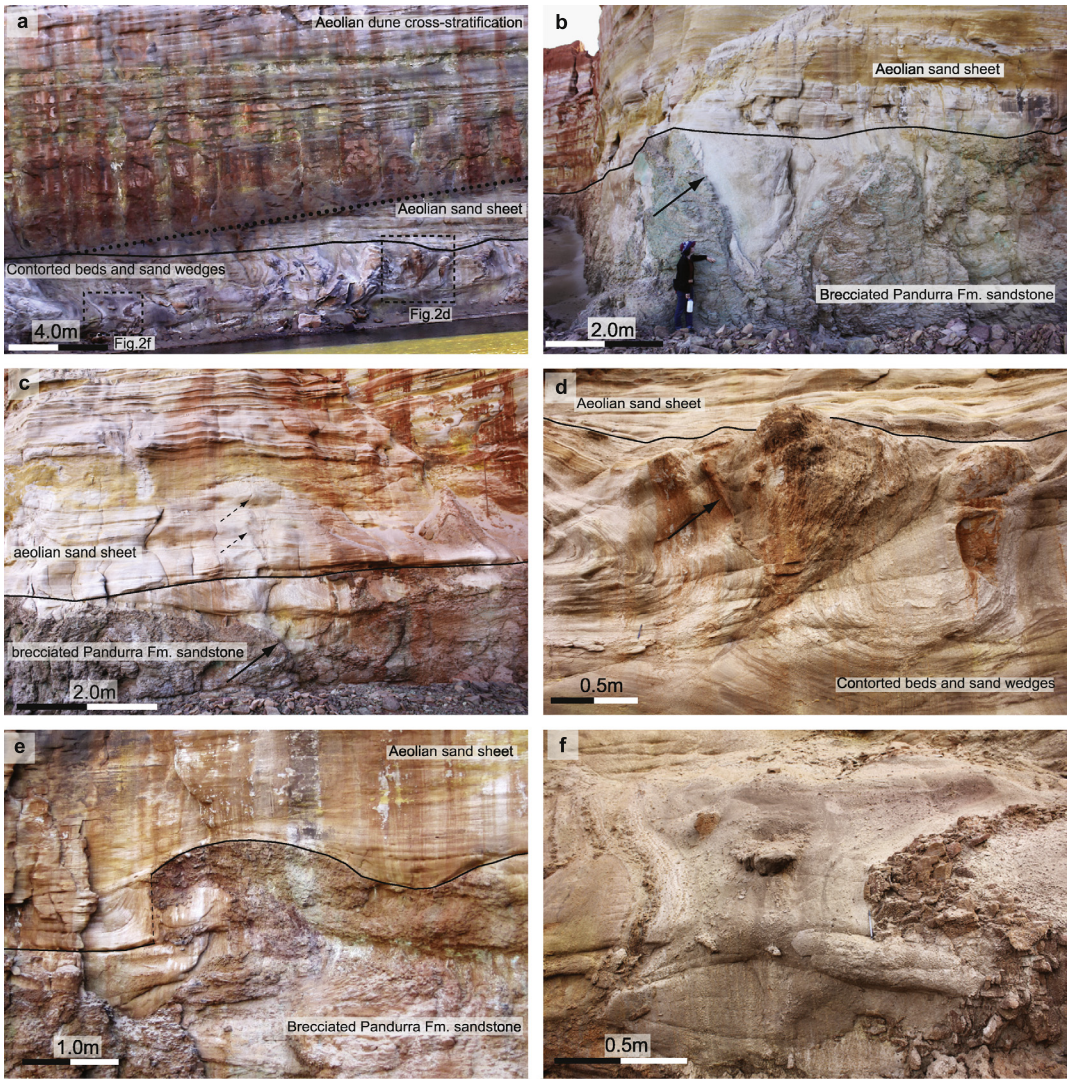

Fig. 4. Photographs of periglacial structures within the Mt. Gunson Mine in South Australia. (a) Contorted bedding and involutions extends 4 m below paleoground surface (black line). Stippled line is dune–sand sheet contact. (b) Epigenetic or anti-syngenetic sand wedge at contact between the Cattle Grid Breccia and sand sheet. Solid black arrow indicates wedge margin. (c) Syngenetic sand wedges indicate sand sheet aggradation at the time of wedge formation. Wedges indicated by dashed black arrows (d) Epi or anti-syngenetic sand wedge. Left side parallels limb of fold indicating synchronous formation. (e) Diapiric structure protruding into overlying sand sheet. Note upturned and onlapping sand sheet strata on either side of the diapir axis. (f) Periglacial involution. Flat base implies an impermeable layer, such as the permafrost table.

raphy along this surface and reveal that this lag surface is the paleoground surface (Fig. 4e). Within the overlying sand sheet facies in the NE Pit, nested, syngenetic sand wedges (Fig. 4c) record a continuity of periglacial features during aggradation of the aeolian sand sheet. Sand wedges within the overlying sand sheet and dune facies are developed on internal bounding surfaces throughout and not along clearly defined horizons previously described and interpreted to represent generations of sand wedges related to long-term climatic oscillations (Williams and Tonkin, 1985; Williams, 1998). This is consistent with our observations outside of the mine where sand wedges are found throughout the Whyalla Sandstone aeolian stratification on set bounding surfaces.

In contrast to the brittle deformation and frozen ground recorded by the sand wedges, a wide range of sedimentary structures indicate ductily deformed sediments – including convolute bedding (Fig. 4, a and d), periglacial involutions (Fig. 4f), and diapiric structures (Fig. 4e) (Sharp, 1942; Swanson et al., 1999; Williams and Tonkin, 1985; Williams, 2007). The convolute bedding appears to be coeval with the growth of the sand wedges, whereby the host strata are progressively deformed as the wedge expands with each crack and fill cycle. The synchroneity of the sand wedges and the collocated contorted beds is demonstrated by the wedge position within the nexus of isoclinal folds of the contorted bedding (Fig. 4d). The minimal deformation of the wedges and the absence of a second, superimposed generation of folds preclude the formation of the wedges pre- or post-deformation.

The involutions and diapiric structures could be interpreted as part of an overall permanently frozen suite of structures that lie below the permafrost table and form coincident with the wedges, or they could be interpreted to form with seasonal freeze and thaw processes that would deform the ground. In the latter scenario, the depth of the involution would indicate the top of the permafrost table (Vandenberghe, 2013), and the base of the active layer, which is 4 m below the paleosurface. Typically, however, involutions of this scale are thought to relate to degrading permafrost on time scales longer than seasonal (Vandenberghe, 2013). The diapiric structures are likely formed by frost heave, but could be part of a thaw cycle.

Prior work by Williams and Tonkin (1985) in a now in-filled Mt. Gunson Mine pit revealed a similar suite of periglacial structures. Williams and Tonkin (1985) interpret many of the defor-

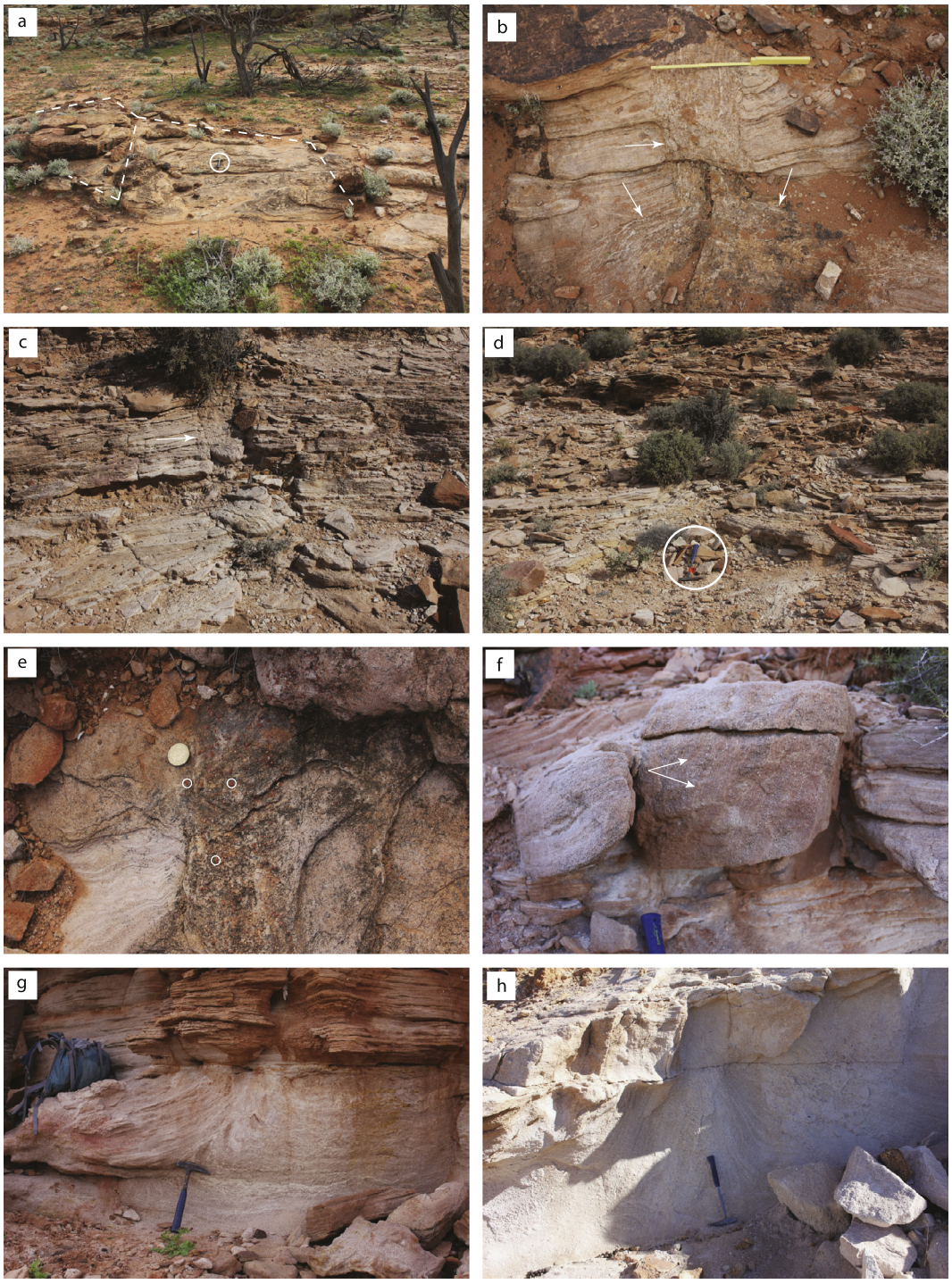

Fig. 5. Sand wedges formed within the Whyalla Sandstone on the Stuart Shelf outside of the Mt. Gunson Mine. (a) Planview of polygonal wedge structure at Whittita locality. Dashed white line outlines the polygonal wedge. (b) Planview of intersection of polygonal sand wedge approximately 40 cm in width at Whittita locality. Folding measuring stick is 60 cm in length. (c) Crossectional view of sand wedge formed in wind ripple stratification noted by the parallel lamination at Whittita locality. White arrow points to edge of the sandwedge truncating the wind ripple lamination. Bleached appearance of sandstone is typical of localities with abundant sand wedges around the Stuart Shelf. (d) Highly sand wedge fractured outcrop at Whittita. Hammer along axis of fracture. Note upturned bedding along sides of wedge. The rock hammer circled in white lies at the center of the wedge. (e) Sand wedge with granules (circled in white) composing interior. Coin sits at the edge of the wedge and wind ripple laminae. (f) Sand wedge at Island Lagoon locality. Note the upturned bedding along the edges of the wedge and the vertical laminae in the interior of the wedge (white arrow). (g) Deformed sandstone at Island Lagoon truncated and overlain by wind ripple stratification. (h) Deformed sandstone at Island Lagoon.

mation structures to form by liquefaction and freeze–thaw action, and they go on to determine a paleoactive layer depth of around 2 m (Williams, 2007). Their interpretation was used in support of severe seasonal climatic amelioration related to Williams (1975) high-obliquity hypothesis. Although involutions and diapirs have also been widely interpreted as indicators of surface melt within an active layer in the literature describing Holocene and Pleistocene periglacial horizons (Sharp, 1942; Swanson et al., 1999), the colocation of these structures along the same stratigraphic horizon as the sand wedges, which are thought to require permanently frozen ground to form, is difficult to explain. Given the challenges associated with interpreting a paleoactive layer, in our discussion

of paleotemperatures we explore the implications for both entirely frozen ground and the active layer model.

3.2. Stuart Shelf sand wedges

Outcrop of the Whyalla Sandstone across the Stuart Shelf is limited, but every outcrop studied contained sand wedges (Fig. 5). Sand wedges in localities outside of the Mt. Gunson mine were not identified in previous studies of the Whyalla Sandstone (Preiss, 1987; Williams, 1998).

Sand wedges outside of the Mt. Gunson mine bear resemblance to narrow syngenetic sand wedges formed within the aeolian sand sheet and dune cross stratified facies of the mine, as well as to Cryogenian sand wedges reported in Mali, West Africa (Deynoux, 1982). The sand wedges range in width from 2 to 120 cm measured orthogonal to the axial plane of the wedge, and filled with mm-scale internal, vertical laminations. In several localities the wedges could be traced from the maximum width to the point of the wedge taper, and in others, the wedges are better described as sand veins, with minimal apparent taper (Murton and Bateman, 2007). Wedge depths ranged from less than 10 cm to greater than 150 cm. Sand wedges outside of the mine displayed far less deformation than those within the mine. At the Whittata locality (Fig. 1), sand wedge polygons were exposed in plan-view at the surface with an average polygon diameter of 3 m (Fig. 5a, b).

Sand wedges were consistently found along the first-order bounding surfaces of the aeolian stratification and within thick packages of wind ripple stratification that compose the base of the majority of the dune sets we studied. We interpret the thick basal wind rippled packages to represent a dune plinth formed under an oblique to longitudinal wind regime (Kocurek, 1991). Wedges are not present in the grainfall and grainflow stratification that comprised the upper portion of the dune sets. Wedge development on the first-order bounding surfaces (Fig. 5a, b, e) and within the wind ripple strata (5c, d, f, g, h) likely reflects the tight sand grain packing associated with the both of these types of strata. Tight grain packing during deposition promotes cementation (Schenk and Fryberger, 1988) – ice formation in this case – which is an essential ingredient for the formation of thermal contraction cracks and wedge development. In contrast, grainfall and grainflow strata are more loosely packed when deposited, more poorly cemented, and are thus less likely to develop thermal contraction fractures. The largest wedges tended to develop along first-order bounding surfaces indicating long exposure times and the stability of these surfaces, and the smaller wedges formed within the more mobile, wind ripple strata of the plinth. The absence of the sand wedges within the grain fall and grain flow strata may also reflect the degree of activity of the dune during the time of wedge formation, where dune avalanching and grainfall events would outpace seasonal ice cementation.

The widespread presence of sand wedges within aeolian strata outside of the Mt. Gunson mine highlights the continuity of active aeolian processes during cold climate conditions. The aeolian activity points to the absence of an entirely frozen regolith or a land surface that was buried in snow or ice. If ground ice was present, climate alternated between periods of freezing and some degree of surface thaw that would allow aeolian transport to occur or severely dry conditions in which little ice would have accumulated on the surface. The significance of the degree of deformation in sand wedges is not well understood, but the minimal deformation observed in the sandsheet and dune facies may relate to the packing of the sand and the amount of pore ice, where greater open pore space and less ice can accommodate wedge expansion without significant deformation (Murton et al., 2000). This could indicate an overall dryer climate than was present during the formation of the highly deformed sand wedges at the base of the mine, which likely formed under constant ice saturation or in the presence of water. Alternatively, the change in wedge type may reflect spatial variability in the local paleogeography, where conditions at the Mt. Gunson Mine promoted ice formation more readily than elsewhere on the Stuart Shelf, perhaps by proximity to a glacial system, water table, or a fluvial or marine system.

3.3. Fluvial deposits

Two outcrop localities within our study area of the Whyalla Sandstone show the juxtaposition of fluvial and periglacial activity. These localities are near Pernatty Lagoon, 9 km due south of the Mt. Gunson Mine (31°31′42.17″S, 137°8′46.21″E), and at Island Lagoon and Lake Finniss, 50 km west of the mine (31°38′5.20″S, 136°40′1.48″E). The most recent and widely accepted interpretation of the Whyalla Sandstone is a cold climate periglacial, aeolian sand sheet (Williams, 1998). However, our observations suggest a reinterpretation of the Whyalla Sandstone as a glacio–fluvial–aeolian formation.

The outcrop south of the Mt. Gunson Mine covers less than a square kilometer and displays a key stratigraphic relationship between a periglacial facies, similar to those recognized in the Mt. Gunson Mine, and the newly recognized fluvial facies. The base of the outcrop is characterized by sand wedges formed within an extensively deformed sandstone that contains subangular, pebble to cobble-sized clasts of Pandurra Formation (Figs. 6 and 7a). The interior of the wedge has vertical laminations and is surrounded by deformed beds with a crinkled texture that appears to be deformed ripple cross-lamination (Fig. 7a). The convolute bedding gives way upward into flat lying crinkled bedding composed of discontinuous, subparallel laminations formed of medium to very coarse, very well-rounded, highly spherical sand grains. The crinkled beds with subparallel laminations also appear to contain deformed ripple cross-lamination. Pebble-sized clasts of Pandurra appear within the crinkled bedding and decrease in concentration upward. The crinkled bedding gives way upward to planar bedding and ripple cross-lamination formed within the same medium to very coarse sandstone and absent the clasts of Pandurra. Although most of the ripple cross lamination appears to be formed by the migration of asymmetrical bedforms indicating unidirectional flow (Fig. 7b), a single instance of symmetrical ripple forms (Fig. 7c) may indicate oscillatory flow from wave action and a different paleoenvironment. The sands that compose the planar bedding and ripples are similar in size and shape to those within the sand wedges and convolute bedding, indicating fluvial reworking of poorly consolidated sands of the sand wedge and convolute facies. The highly spherical grains suggest aeolian cycling of the sand.

The upper portion of the outcrop south of the Mt. Gunson Mine is characterized by dune cross stratification ranging between 20 and 60 cm set thickness formed in a medium to coarse sandstone (Fig. 7d). Tabular and trough cross-stratified beds are truncated laterally by channels ranging up to 3 m in depth and 20 m in width and composed of dune trough cross stratification with cobble to boulder size angular clasts of Pandurra Formation at the base of the channels (Fig. 7e). Paleocurrent analysis indicates the overall transport direction of the fluvial system was toward the south with a mean resultant paleotransport direction of 202°. Despite the clear indicators of unidirectional currents, a single instance of symmetrical ripple forms indicating oscillatory flow were found and may indicate wave action in a standing body of water. A laterally discontinuous 20–50 cm thick pebble to cobble conglomerate caps the sequence (Fig. 7f, g, h). The cobble clasts are nearly all very well-rounded and composed of megaquartz dissimilar to the clasts of Pandurra Formation found within the channels or at the base of the section. A single striated cobble (Fig. 7g) was found among

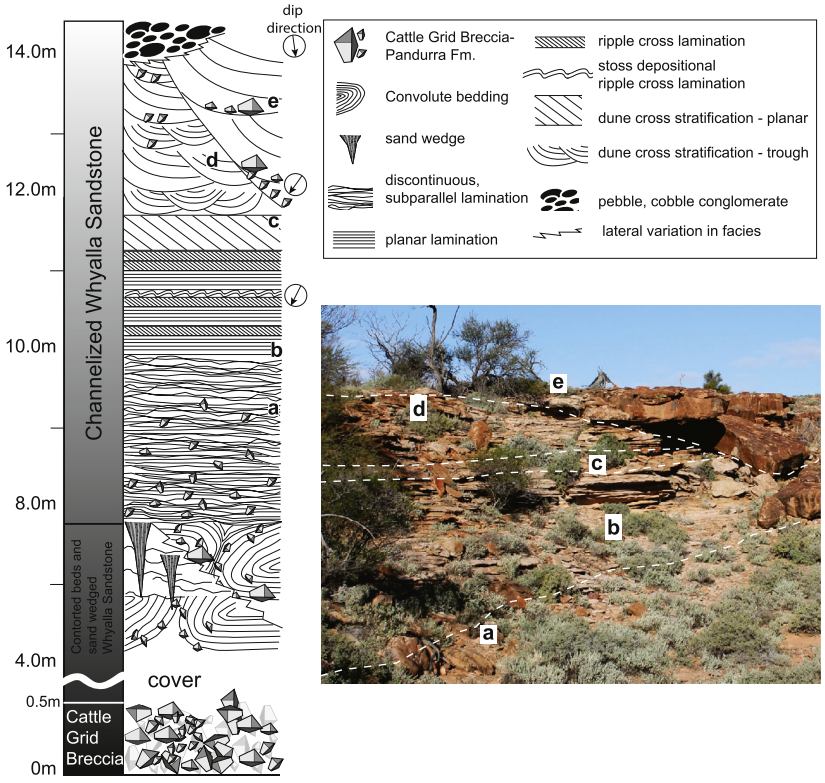

Fig. 6. (a) Composite stratigraphic section of sand wedge, deformed strata and fluvial facies of Whyalla Sandstone near Pernatty Lagoon. Dip direction arrows show measurements from ripple forms and ripple and dune cross-stratification ($n = 68$). Dip direction is corrected for paleogeographic configuration and indicates an overall southern transport direction. (b) Photograph of one section of the fluvial facies. Letters in the photo indicate the different facies in the photograph and match those shown in the stratigraphic column. Note the prominent channel (e) cuts through the dune and ripple facies.

the conglomerate, indicating the cobbles may have been part of a nearby glacial system.

The outcrops at Island Lagoon and Lake Finniss do not exhibit the channelized fluvial facies, but rather have two distinct packages of low-angle and trough cross-stratification formed in a medium to very coarse, very well-rounded, highly-spherical, poorly cemented subarkose sandstone. No Pandurra clasts are found in this area: the deformation is entirely within the Whyalla Sandstone. The low-angle cross-stratification at Island Lagoon was originally interpreted as an aeolian sand sheet (Williams, 1998). However, asymmetrical fluvial ripples and dune-scale sets formed in coarse to very coarse grained sand found in the outcrops indicate that at least some of the outcrop is fluvial, although we could not eliminate the possibility that other areas of the outcrop were aeolian. The outcrop is separated by two erosional surfaces marked by truncated dune-scale cross sets, some of which appear fluvial in origin, as well as sand wedges and convolute bedding. Typically, only the lower, tapering portion of the sand wedges and upturned deformed strata are preserved. The erosional contacts are sharp and uniform in elevation across the outcrop. The upper erosional surface marks the top of the outcrop and is highly silicified. The origin of the erosional surface is not clear and could indicate fluvial erosion down to a permafrost table, aeolian deflation, or a glacial surface, though no other glacial-like features are found along these horizons.

4. Discussion

4.1. Sand wedge formation and models to explain low-latitude sand wedges

One of the paleoclimate centerpieces in the South Australia Marinoan sedimentary record that can be used to constrain paleotemperatures is periglacial sand wedges surrounded by deformed ground (Fig. 2). Sand wedges are widespread in Cryogenian (720–635 million years ago) sedimentary successions in West Africa (Deynoux, 1982), Norway (Edwards, 1975), Scotland (Spencer, 1971), and South Australia (Figs. 2, 4a–f, 5a–h) (Williams and Tonkin, 1985). The sand wedges in South Australia, however, are the only reported Cryogenian sand wedges developed at less than 30° paleolatitude (Hoffman and Li, 2009), and cannot be explained readily using modern high-latitude analogs where seasonal temperature variations are extreme.

In an effort to explain South Australian sand wedges and the wide-spread glacial deposits at the paleoequator, Williams (1975, 2007) developed the prominent precursor to the snowball Earth hypothesis, the high-obliquity hypothesis (Schmidt and Williams, 1995; Williams et al., 1998; Williams, 2007, 1975). This hypothesis purported that during the Precambrian, Earth's obliquity (i.e., the angle between the Earth's axes of rotation and its axis of orbit around the sun) was greater than 54°, as compared with about 23° today, and this configuration allowed mean annual temperatures at the equator to drop below 0 °C. Importantly, this would have increased equatorial seasonality, thereby allowing sand wedge growth. Based on the presence of sand wedges and the temperature regime within which sand wedges form today, Williams and Tonkin (1985) suggested a temperature range from −20 °C to +4 °C. Criticisms of the high-obliquity model highlight the absence of an explanation for the meridional distribution of the entire suite of Precambrian climate-sensitive rocks, including evaporites and the Cryogenian pre- and post-glacial carbonates (Evans, 2006), and for a rapid shift of Earth's obliquity between Cryogenian and Cambrian times (Hoffman and Li, 2009), when Earth's orbital configuration is better constrained.

The South Australian wedges also engendered a potential challenge to a snowball Earth climate state because strong equatorial

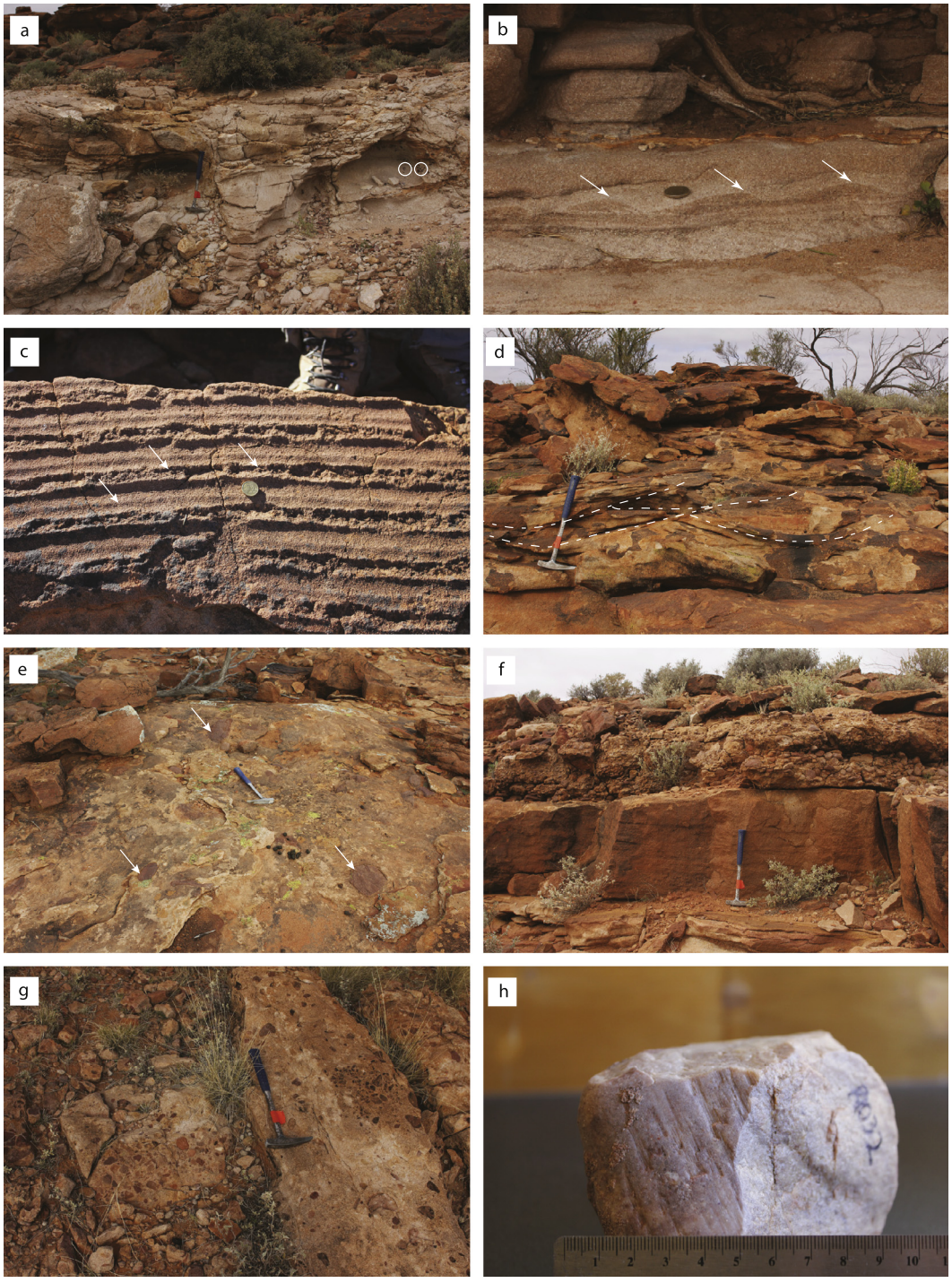

Fig. 7. Sand wedge, deformed strata, and channelized facies of Whyalla Sandstone near Pernatty Lagoon. (a) Sand wedge and deformed strata overlain by channelized facies. Wedge and deformed strata are highly altered denoted by bleached color. Overlying channelized facies are dark and oxidized. Note clasts of Pandurra Formation within wedge circled in white. (b) Asymmetrical, stoss-depositional ripple cross-lamination (white arrows indicate ripple crests). (c) Symmetrical ripple forms (crest indicated by white arrows). (d) Dune trough cross-stratification. Dashed white lines highlight troughs. (e) 20–30 cm subangular boulders (indicated by white arrows) within structureless sand. (f) Well-rounded cobble conglomerate capping sandy dune facies. (g) Cobbles within sandstone. (h) Striated cobble found within conglomerate.

seasonality would not be expected for a modern orbital configuration (Hoffman and Li, 2009; Hoffman and Schrag, 2002). This was partially reconciled by a low-latitude sand wedge hypothesis with a model proposing that thermal contraction fractures, a key ingredient of sand wedges, could form under snowball-Earth conditions by diurnal temperature fluctuations (Maloof et al., 2002). In this hypothesis, diurnal temperature swings drive thermal contraction cracking in the upper decimeter or so of the ground, and because the regolith is sufficiently cold and brittle at snowball Earth temperatures, fractures propagates to several meters depth. Although temperatures predicted by a snowball Earth climate could generate brittle ground and allow cracking at several meters depth by diurnal temperature oscillations, the cold temperatures and brittle ground also preclude the formation of ductily deformed ground during sand wedge development over daily time scales, which is inconsistent with our observations.

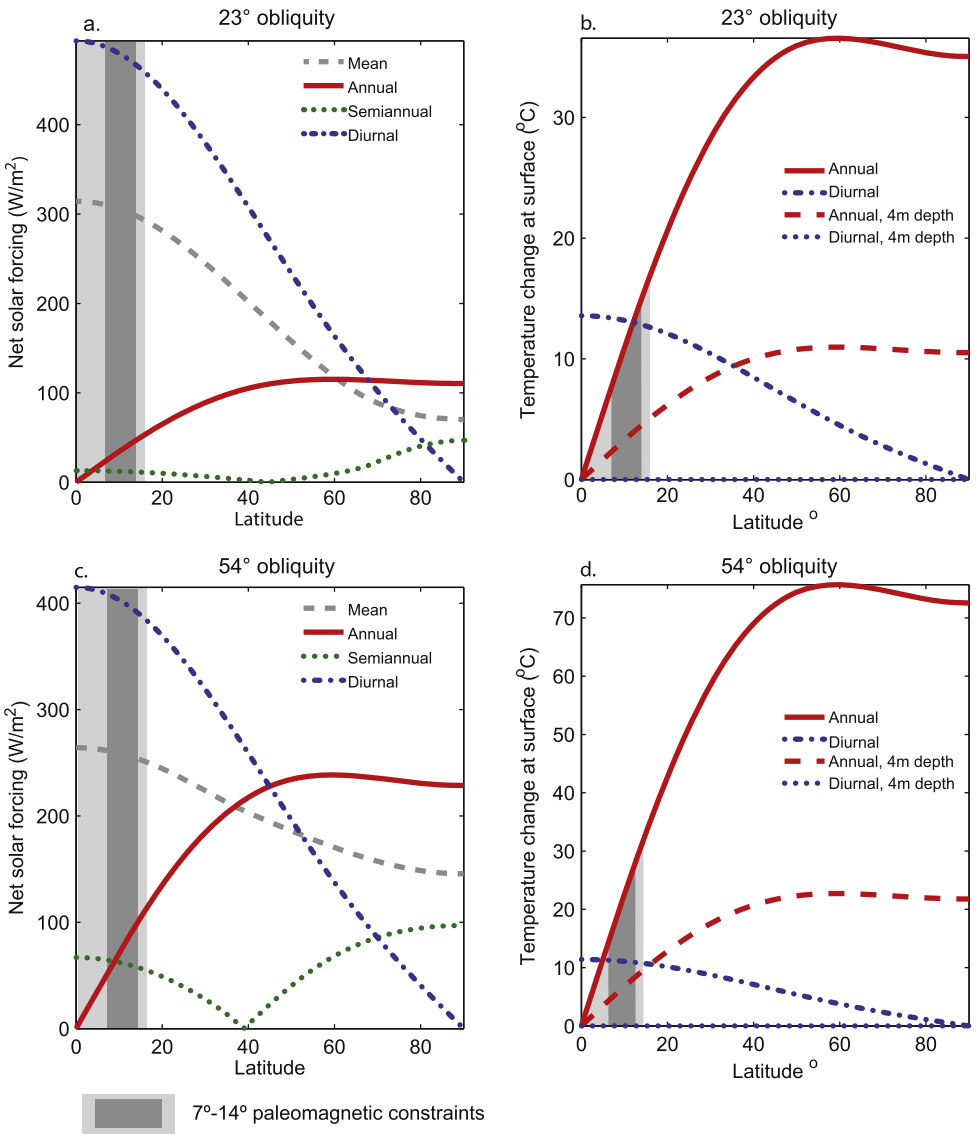

Fig. 8. Idealized thermodynamic model results. (a) Annual-mean net solar forcing and range of variability at annual, semiannual, and diurnal frequencies. (b) Range of temperature variability at surface and at 4 m depth within the regolith at annual and diurnal frequencies. (b, d) As in (a, c) but for obliquity of 54° rather than 23.4°. The model is described in the Supplementary Material. The temperature variability at depth assumes a dry sandy regolith. Plotted values for each frequency are the range between the maximum and minimum values in the cycle, i.e., two times the amplitude of variability. Dark gray bars show range of paleomagnetic constraints on paleolatitudes, and light grey area shows approximate range of minimum and maximum errors on the range of measurements.

4.2. Model of ground temperatures

Current models to explain low-latitude wedges are fundamentally built upon an assumption that seasonal temperature fluctuations near the equator in the modern orbital configuration are insufficient for sand wedges to form (Maloof et al., 2002; Williams and Tonkin, 1985). Here we relax this constraint and explore temperature fluctuations near the equator to better understand the range of expected temperatures associated with low-latitude wedge formation. The two most likely mechanisms to produce the repeated temperature oscillations within the ground are solar-forced (1) diurnal and (2) annual temperature fluctuations with the expectation that at the equator diurnal temperature variations are the strongest and the annual temperature variations are weaker.

We apply a simple thermodynamic model of the atmosphere and underlying regolith with solar insolation forcing that varies as a function of latitude and examine the resulting patterns of temperature variability within the ground for both the current and high-obliquity scenarios. The model is described in the Supplementary Material. It includes surface temperatures computed assuming a linear response to solar insolation and thermal diffusion within the sandy regolith below. The model results illustrate that the original notion that seasonality at the paleolatitude of the sand wedges was weak for the current 23.4° obliquity (Williams, 2007, 1975), which motivated both the high-obliquity hypothesis and diurnal-mechanism, applies only to a narrow range of latitudes near the equator (Fig. 8). The annual cycle in surface temperature rapidly strengthens away from the equator, and it exceeds the amplitude of the diurnal cycle, even at the ground surface, for latitudes greater than about 12° latitude (Fig. 8b, d). Heat diffuses into the regolith to a characteristic depth of ~3 m for the annual cycle, compared with 20 cm for the diurnal cycle, suggesting that at all latitudes the temperature variability is primarily annual at the meter-scale depths where the sand wedges and deformation structures are found. Fig. 8c and d demonstrate that a high-obliquity Earth would generate strong seasonal temperature variations at the equator sufficient for sand-wedge formation. However, in comparison, the calculation also demonstrates that the expected

temperature ranges under a normal orbital configuration provide a reasonably high temperature change for the constrained paleolatitudes, and the high-obliquity scenario is not a necessary condition.

These calculations demonstrate that if only diurnal temperature variations are considered (Fig. 8b, d), the ground at meter-scale depths would remain virtually isothermal and brittle under the cold snowball Earth conditions (Maloof et al., 2002). The absence of temperature variability at meter-scale depths in brittle ground does not allow for the formation of the ground deformation we observe associated with the wedges, limiting the efficacy of the diurnal model for the full suite of periglacial features in the South Australia Cryogenian succession.

If the tropical paleolatitude is broadly correct, we hypothesize that the wedges can still be explained by the annual temperature cycle, which is at least as strong as the diurnal cycle at the surface and propagates far deeper within the ground. We calculate the maximum annual temperature change within the range of paleolatitudes of the Whyalla Sandstone to be about 8 °C (Fig. 8b). These temperature ranges match approximately that of today at the same latitudes. Given the damping of temperature oscillations with depth, we calculate the annual temperature range at 4 m depth, which is the depth to which we observe ground deformation, to be around 2.5 °C (Fig. 8b). The stresses induced by such a small temperature change in frozen ground at temperatures suggested previously (−20 °C or colder) are unlikely to be sufficient to deform the ground surrounding a sand wedge. Thus, we propose the alternative hypothesis that temperatures must have been warmer than currently estimated to allow ductile deformation of frozen ground. Minimally, this places temperatures at 4 m depth at the brittle–ductile transition of an ice–rock mixture. Although the temperature at which this occurs depends on a range of the ice–rock mixture properties, ice–rock mixtures tend to increase regolith brittleness at warmer temperatures, as compared to pure ice, thereby raising the minimum temperature at which ductile deformation can occur. The severity of the deformation we observe would be most easily accomplished if partial melt was present in the ground, which could occur with the seasonal formation of segregation ice or freeze and thaw of an active layer. If the ground were to annually cross the melting point at several meters depth, our calculations highlight that mean annual surface temperatures would be within a few degrees of 0 °C. This temperature estimate also readily explains our observations of fluvial deposits generated by surface runoff.

4.3. Fluvial activity during the Marinoan glaciation

The presence of an active fluvial system within the Whyalla Sandstone places an important constraint on the climate during the Marinoan glaciation. Temperatures were sufficiently warm to allow surface runoff in at least two localities. In one locality, near the Mt. Gunson Mine, the fluvial system had well-developed channels and transported boulder-sized clasts. At another, near Island Lagoon and Lake Finniss, distinct erosional horizons mark the alternation of periglacial processes and aeolian and fluvial activity. In another interpretation, the fluvial component of the Whyalla Sandstone could arise from subglacial melt, but direct evidence of glacial activity is limited to the Elatina Formation and not found on the Stuart Shelf. Importantly, all of this activity was occurring prior to deposition of the post-glacial Nuccaleena Formation cap carbonate and constrains this activity to have been part of the Marinoan glacial interval.

The presence of surface runoff could be interpreted as seasonal or longer-term climatic amelioration during a dominantly glacial interval. If seasonal, the runoff suggests temperatures at least rose above the melting point long enough during the summer for well-evolved fluvial system to develop. Based upon our temperature calculations, this constrains minimum mean annual surface temperatures to be −8 °C, in order to allow temperatures to cross the melting point. This temperature is consistent with ground ice being sufficiently ductile for the development of the deformation we observe. If the fluvial deposits are related to flooding events, the outcrop at Pernatty Lagoon is difficult to explain because of the absence of a significant erosional horizon between the periglacial and fluvial contact. A flood may better explain the erosional surfaces at Island Lagoon, but larger clasts that might be expected with a flood are absent. Lastly, the fluvial deposits may indicate intervals of widespread warming during the glaciation, which could imply that part of the Cryogenian had a style of glaciation similar to that of the Pleistocene in which temperatures oscillate between warm and cool on tens-of-thousands of year timescales.

Though stratigraphic relationships place the fluvial activity within the Whyalla Sandstone, this activity could have occurred before or after peak glaciation as reported elsewhere for fluvial and deltaic deposits in the Elatina Formation (Le Heron et al., 2011; Rose et al., 2013; Williams et al., 2008). If the deposits are generated by climatically-driven warming and occur pre- or post-glacial, then the punctuated periglacial and fluvial activity records temperature oscillations, rather than continuous rapid glacial onset or deglaciation. Alternatively, the fluvial activity could be explained by the spatial variations in local environments occurring within a dynamic glacial outwash system in which sand dunes, fluvial environments, and periglacial environments co-existed. If this occurred prior to peak glaciation, then there is no record of the peak glaciation or post-glacial environment prior to deposition of the Nuccaleena Formation. If part of the post-glacial sequence, then deglaciation in South Australia was cold enough for sand wedges to form and occurred over a time-scale that allowed the development of fluvial systems and the accumulation of nearly two hundred meters of aeolian sediments.

4.4. Implications for snowball Earth hypothesis

If the Whyalla Sandstone spans part of the peak Marinoan glacial sequence as others have suggested (Williams et al., 2008), our observations imply that the Marinoan glaciation in South Australia was less severe than suggested by the snowball Earth hypothesis. We explore a range of implications for the snowball Earth hypothesis below:

1. Ice did not cover the land surface during the time the wedges formed and the dunes were active. Though models and geologic evidence differ on the amount of ice and snow accumulation at the equator (Hoffman, 2011; Pierrehumbert, 2002; Pierrehumbert et al., 2011), ice sheets are thought to cover all continents (Hoffman, 2011). Our observation is compatible with Williams (2007), who also highlights the presence of dunes and sand wedges as evidence of an ice-free land surface.

2. Surface water was present in sufficient quantities for a well-developed fluvial channels to form on the Stuart Shelf. This observation is incompatible with the snowball Earth climate, in which the hydrologic cycle is minimal and no significant surface runoff is present. The association of the channel deposits with the wedge-generated convolute bedding suggests an ongoing cold climate associated with surface melt. The runoff may be associated with the presence of a nearby glacier indicated by the striated clast found in one locality. These observations also highlight that the Whyalla Sandstone should be re-evaluated as a glacio–fluvial–aeolian formation and not only periglacial–aeolian formation, as proposed by Williams (1998). Our paleoenvironmental interpretation is similar to what was envisioned by Preiss (1987) in his reconstruction of the Stuart Shelf and implied by others in their discussion of the fluvial component to the Elatina Formation (Le Heron et al., 2011; Rose et al., 2013).

3. Temperatures were warm enough for ground ice to deform ductily, which provides a temperature constraint for the Whyalla Sandstone. A temperature near 0 °C is higher than predicted in the current snowball model and inconsistent with most GCM simulations of snowball Earth conditions (Pierrehumbert et al., 2011). This temperature is compatible with temperature estimates of the variants on the snowball Earth including the slushball models (Abbot et al., 2011; Peltier et al., 2007). The periglacial diapirs and involutions we observe could form within an active layer or degrading permafrost conditions indicating that freeze-thaw or melting may have occurred to several meters depth. Our estimates of an active layer are consistent with Williams (2007), who reports the presence of a 2 m active layer and widespread melt structures. Given the equatorial paleolatitude constraint, our calculations indicate that with paleoactive layer depth ranging from 2 to 4 m, mean annual surface temperatures would have been within 2 and 5 °C.

5. Conclusions

The geological observations of periglacial structures – sand wedges, convolute bedding, involutions and diapiric structures – indicate that the ground was sufficiently warm to ductily deform or melt during the Marinoan Glaciation. These observations, paired with a model of annual ground temperature change in the low latitudes, narrows the bounds on the range of environmental conditions expected during the Marionan Glaciation in South Australia. Temperature estimates around 0 °C match well with the occurrence of fluvial deposits associated with the periglacial structures and indicate that significant melt was present on the land surface during the glaciation. The presence of fluvial deposits in several localities on the Stuart Shelf, along with wide-spread periglacial and aeolian deposits, point to an environment like a sandy braid plain that may have drained a nearby glacial environment. Although the Whyalla Sandstone has long been considered as part of the peak Marinoan Glacial suite, there is insufficient outcrop to link the Whyalla Sandstone with the Elatina Formation and place definitive bounds on the timing. Despite this, the facies present and our temperature calculations show that South Australia during the Marinoan Glaciation was one of the coldest tropical climates in Earth's history and highlight the need for more geological constraints of temperature to constrain the glacial severity during the Cryogenian Period.

Acknowledgements

This material is based upon work supported by the National Science Foundation (EAR-PF-0846233 to R.C.E., EAR-1053523 to W.F., EAR-0842946 to A.C.M., and ARC-1107795 to I.E.). M.L. acknowledges support from the donors of the American Chemical Society Petroleum Research Fund and the Terrestrial Hazard Observations and Reporting center at Caltech. Catherine V. Rose provided useful discussion of the geologic observations. We thank A. and M.J. Musolino Pty Ltd. for access to the Mt. Gunson Mine. Daniel Le Heron and Ryan McKenzie provided insightful comments that improved this study.

Appendix A. Supplementary material

Supplementary material related to this article can be found online at http://dx.doi.org/10.1016/j.epsl.2014.09.017.

References

Abbot, D.S., Voigt, A., Koll, D., 2011. The Jormungand global climate state and implications for Neoproterozoic glaciations. J. Geophys. Res. 116, 1–14.
Allen, P.A., Etienne, J.L., 2008. Sedimentary challenge to snowball Earth. Nat. Geosci. 1, 817–825.
Black, R.F., 1976. Periglacial features indicative of permafrost: ice and soil wedges. Quat. Res. 6, 3–26.
Bowring, S.A., Grotzinger, J.P., Condon, D.J., Ramezani, J., Newall, M.J., Allen, P.A., 2007. Geochronologic constraints on the chronostratigraphic framework of the Neoproterozoic Huqf Supergroup, Sultanate of Oman. Am. J. Sci. 307, 1097–1145.
Condon, D.J., Zhu, M., Bowring, S.A., Wang, W., Yang, A., Jin, Y., 2005. U–Pb ages from the Neoproterozoic Doushantuo Formation, China. Science 308, 95–98.
Crowley, T.J., Hyde, W.T., Richard, W., 2001. CO_2 levels required for deglaciation of a "near-snowball" Earth. Geophys. Res. Lett. 28, 283–286.
Deynoux, M., 1982. Periglacial polygonal structures and sand wedges in the late Precambrian glacial formations of the Taoudeni basin in Adrar of Mauretania (West Africa). Palaeogeogr. Palaeoclimatol. Palaeoecol. 39, 55–70.
Edwards, M.B., 1975. Glacial retreat sedimentation in the Smalfjord Formation, Late Precambrian, North Norway. Sedimentology 22, 75–94.
Evans, D.A.D., 2006. Proterozoic low orbital obliquity and axial-dipolar geomagnetic field from evaporite palaeolatitudes. Nature 444, 51–55.
Evans, D.A., Raub, T.D., 2011. Neoproterozoic glacial paleolatitudes: a global update. In: Arnaud, E., Shields, G., Halverson, G.P. (Eds.), The Geological Record of Neoproterozoic Glaciations. Geological Society of London. 752 pp.
Hallet, B., Sletten, R., Whilden, K., 2011. Micro-relief development in polygonal patterned ground in the Dry Valleys of Antarctica. Quat. Res. 75, 347–355.
Harland, W.B., 2007. Origins and assessment of snowball Earth hypotheses. Geol. Mag. 144, 633–642.
Hoffman, P.F., 2011. Strange bedfellows: glacial diamictite and cap carbonate from the Marinoan (635 Ma) glaciation in Namibia. Sedimentology 58, 57–119.
Hoffman, P.F., Li, Z.-X., 2009. A palaeogeographic context for Neoproterozoic glaciation. Palaeogeogr. Palaeoclimatol. Palaeoecol. 277, 158–172.
Hoffman, P.F., Schrag, D.P., 2002. The snowball Earth hypothesis: testing the limits of global change. Terra Nova 14, 129–155.
Hoffman, P.F., Kaufman, A.J., Halverson, G., Schrag, D., 1998. A Neoproterozoic snowball earth. Science 281, 1342–1346.
Hoffmann, K.-H., Condon, D.J., Bowring, S.A., Crowley, J.L., 2004. U–Pb zircon date from the Neoproterozoic Ghaub Formation, Namibia: constraints on Marinoan glaciation. Geology 32, 817–820.
Kirschvink, J.L., 1992. Late Proterozoic low-latitude global glaciation: the snowball earth. In: Schopf, J.W., Klein, C. (Eds.), The Proterozoic Biosphere. Cambridge University Press, Cambridge, pp. 51–52.
Kocurek, G., 1991. Interpretation of ancient aeolian sand dune. Annu. Rev. Earth Planet. Sci. 19, 43–75.
Kocurek, G., Havholm, K.G., 1993. Eolian sequence stratigraphy – a conceptual framework. In: Weimer, P., Posamentier, H.W. (Eds.), Siciliclastic Sequence Stratigraphy. In: AAPG Mem., pp. 393–409.
Le Heron, D.P., Cox, G., Trundley, A., Collins, A.S., 2011. Two Cryogenian glacial successions compared: aspects of the Sturt and Elatina sediment records of South Australia. Precambrian Res. 186, 147–168.
Mackay, J.R., 1990. Some observations on the growth and deformation of epigenetic, syngenetic and anti-syngenetic ice wedges. Permafr. Periglac. Process. 1, 15–29.
Maloof, A.C., Kellogg, J.B., Anders, A.M., 2002. Neoproterozoic sand wedges: crack formation in frozen soils under diurnal forcing during a snowball Earth. Earth Planet. Sci. Lett. 204, 1–15.
McGlown, A., Ewing, R.C., Rose, C.V., 2012. Facies variability in the post-Marinoan cap carbonate Nuccaleena Formation on the Stuart Shelf, South Australia. In: AGU Fall Meeting. p. B13D-0551.
Mellon, M.T., 1997. Small-scale polygonal features on Mars: seasonal thermal contraction cracks in permafrost. J. Geophys. Res. 102, 25617.
Murton, J.B., Bateman, M.D., 2007. Syngenetic sand veins and anti-syngenetic sand wedges, Tuktoyaktuk Coastlands, Western Arctic Canada. Permafr. Periglac. Process. 47, 33–47.
Murton, J.B., Worsley, P., Gozdzik, J., 2000. Sand veins and wedges in cold aeolian environments. Quat. Sci. Rev. 19, 899–922.
Peltier, W.R., Liu, Y., Crowley, J.W., 2007. Snowball Earth prevention by dissolved organic carbon remineralization. Nature 450, 813–818.
Pewe, T.L., 1959. Sand-wedge polygons (tesselations) in the McMurdo Sound Region, Antarctica – a progress report. Am. J. Sci. 257, 545–552.
Pierrehumbert, R.T., 2002. The hydrologic cycle in deep-time climate problems. Nature 419, 191–198.
Pierrehumbert, R.T., Abbot, D.S., Voigt, A., Koll, D., 2011. Climate of the Neoproterozoic. Annu. Rev. Earth Planet. Sci. 39, 417–460.
Preiss, W.V., 1987. The Adelaide Geosyncline – late Proterozoic stratigraphy, sedimentation, palaeontology and tectonics. Bull. - Geol. Surv. S. Aust. 53, 186–196.
Preiss, W.V., 2000. The Adelaide Geosyncline of South Australia and its significance in Neoproterozoic continental reconstruction. Precambrian Res. 100, 21–63.
Rose, C.V., Maloof, A.C., 2010. Testing models for post-glacial "cap dolostone" deposition: Nuccaleena Formation, South Australia. Earth Planet. Sci. Lett. 296, 165–180.
Rose, C.V., Maloof, A.C., Schoene, B., Ewing, R.C., Linnemann, U., Hofmann, M., Cottle, J.M., 2013. The end-Cryogenian glaciation of South Australia. Geosci. Can. 40, 256–293.
Schenk, C.J., Fryberger, S.G., 1988. Early diagenesis of eolian dune and interdune sands at White Sands, New Mexico. Sediment. Geol. 55, 109–120.

Schmidt, P.W., Williams, G.E., 1995. The Neoproterozoic climatic paradox: equatorial palaeolatitude for Marinoan glaciation near sea level in South Australia. Earth Planet. Sci. Lett. 134, 107–124.
Schmidt, P.W., Williams, G.E., McWilliams, M.O., 2009. Palaeomagnetism and magnetic anisotropy of late Neoproterozoic strata, South Australia: implications for the palaeolatitude of late Cryogenian glaciation, cap carbonate and the Ediacaran System. Precambrian Res. 174, 35–52.
Sharp, R.P., 1942. Periglacial involutions in North-Eastern Illinois. J. Geol. 50, 113–133.
Sletten, R.S., Hallet, B., Fletcher, R.C., 2003. Resurfacing time of terrestrial surfaces by the formation and maturation of polygonal patterned ground. J. Geophys. Res. 108, 1–10.
Sohl, L.E., Christie-Blick, N., Kent, D.V., 1999. Paleomagnetic polarity reversals in Marinoan (ca. 600 Ma) glacial deposits of Australia: implications for the duration of low-latitude glaciation in Neoproterozoic time. Geol. Soc. Am. Bull. 111, 1120–1139.
Spencer, A.M., 1971. Late Pre-Cambrian Glaciation in Scotland. Geol. Soc. London Mem. 6, 99.
Sumner, D.Y., Kirschvink, J.L., Runnegar, B.N., 1987. Soft-sediment paleomagnetic fold tests of late Precambrian glaciogenic sediments. Eos (Washington. DC) 68, 1251.
Swanson, D.K., Ping, C., Michaelson, G.J., 1999. Diapirism in soils due to thaw of ice-rich material near the permafrost table. Permafr. Periglac. Process. 10, 349–367.
Vandenberghe, 2013. Cryoturbation structures. In: Elias, S.A., Mock, C.J. (Eds.), Encyclopedia of Quaternary Science. Elsevier Inc., pp. 430–435.
Williams, D.M., Kasting, J.F., Frakes, L.A., 1998. Low-latitude glaciation and rapid changes in the Earth's obliquity explained by obliquity-oblateness feedback. Nature 396, 453–456.
Williams, G.E., 1975. Late Precambrian glacial climate and the Earth's obliquity. Geol. Mag. 112, 441–444.
Williams, G.E., 1998. Late Neoproterozoic periglacial aeolian sand sheet, Stuart Shelf, South Australia. Aust. J. Earth Sci. 45, 733–741.
Williams, G.E., 2007. Proterozoic (pre-Ediacaran) glaciation and the high obliquity, low-latitude ice, strong seasonality (HOLIST) hypothesis: principles and tests. Earth-Sci. Rev. 87, 61–93.
Williams, G.E., Tonkin, D.D., 1985. Periglacial structures and palaeoclimatic significance of a late Precambrian block field in the Cattle Grid copper mine, Mount Gunson, South Australia. Aust. J. Earth Sci. 32, 287–300.
Williams, G.E., Gostin, V.A., McKirdy, D.M., Preiss, W.V., 2008. The Elatina glaciation, late Cryogenian (Marinoan Epoch), South Australia: sedimentary facies and palaeoenvironments. Precambrian Res. 163, 307–331.

Supplementary material for New constraints on equatorial temperatures during a Late Neoproterozoic snowball Earth glaciation

Authors: Ryan C. Ewing[1]*, Ian Eisenman [2], Michael P. Lamb [3], Laura Poppick[4], Adam C. Maloof[4], Woodward W. Fischer[3]

Affiliations:

[1]Department of Geology and Geophysics, Texas A&M University, College Station, TX 77843

[2]Scripps Institution of Oceanography, University of California at San Diego, La Jolla, CA 92093.

[3]Division of Geological and Planetary Sciences, California Institute of Technology, Pasadena, CA 91125.

[4]Department of Geosciences, Princeton University, Princeton, NJ 08544.

* Correspondence to: rce@geos.tamu.edu

Supplementary Material: Model of ground temperature

Here we derive a model that describes the diurnal and annual cycle in temperature at the Cattle Grid Mine site as a function of its paleolatitude during a snowball glaciation. Both geological observations of the sand wedges (Fig. 2) and sedimentary structures indicate the presence of an active aeolian sand sheet and dunes during the development of the wedges, implying that the surface was bare throughout the year. The model describes the temperature at the surface and in the regolith below assuming snow-free surface conditions.

The zonal-mean climate during a snowball glaciation differed from modern conditions due to factors including a smaller thermal inertia associated with ice covering the oceans and a higher surface albedo (Pierrehumbert et al., 2011). Simulations of a snowball glaciation using comprehensive climate models vary substantially depending on how quantities such as surface albedo are parameterized (e.g., Fig. 5 in Pierrehumbert et al., 2011). Here we adopt a simpler approach and assume that the amplitudes of the diurnal and annual cycles in temperature at a location with bare land during a snowball glaciation would be similar to a location with bare land at the same latitude in the modern climate, which is consistent with the range of results for the annual cycle from comprehensive climate models (Pierrehumbert et al., 2011). In order to describe the characteristic meridional structure of modern observed surface temperature variability over land, we use a combination of observed temperature variability and the most salient physics involved with periodic variability that arises from a linear response to solar insolation, drawing on previous energy balance models of Earth's climate (North et al., 1981). This approach focuses only on periodic temperature variability, rather than including a representation of the annual-mean temperature, and it treats the vertical structure in the atmosphere, horizontal energy transport, the planetary albedo, the dependence of outgoing infrared radiation on surface temperature, and the effective heat capacity associated with surface temperature changes as constant. Scalar parameters that describe the heat capacities associated with annual and diurnal variability in the model are derived from observations of modern temperature variability.

Solar insolation

The analytical formula for insolation reaching the Earth as a function of latitude and season is derived in a number of textbooks (e.g., Sec. 2.7 of Hartmann 1994 and Sec. 7.3 of Pierrehumbert 2011), and the relevant points for this discussion are summarized below. We consider a circular orbit because the eccentricity of Earth's orbit is expected to be negligible for the purposes of this model. In this case, the insolation is

$$S(t) = \begin{cases} S_c[\sin\phi\sin\delta + \cos\phi\cos\delta\cosh] & -h_0 < \mathrm{mod}(h+\pi, 2\pi) - \pi < h_0 \text{ [day]} \\ 0 & \text{otherwise [night]} \end{cases}. \quad (1)$$

Here $S_c = 1285$ Wm^{-2} is the solar constant (94% of its present value), ϕ is latitude, δ is the declination angle (latitude of the point on Earth's surface directly under the sun at noon), h is the hour angle (longitude of the subsolar point relative to its position at noon), and h_0 is the hour angle at sunset (with $-h_0$ being sunrise). The declination angle is computed from

$$\sin(\delta) = \sin(\varepsilon)\sin(\lambda) \quad (2)$$

with being obliquity and λ being the solar longitude of Earth's orbit (angle between vernal equinox and the position in Earth's orbit). We use the modern value of obliquity by default, $\varepsilon = 23.4^\circ$, and

we also consider a high-obliquity world with $\varepsilon = 54^\circ$. For a circular orbit, λ varies at a uniform rate during the course of the year. The hour angle at sunset is computed from

$$\cos(h_0) = -\tan(\phi)\tan(\delta) \tag{3}$$

except when $|\phi| \geq \frac{\pi}{2} - |\delta|$, which occurs during polar day and polar night. In this case, when ϕ and δ have the same sign (polar day) we use $h_0 = \pi$ and otherwise (polar night) we use $h_0 = 0$. We use a measure of time (t) that is normalized by the diurnal period, i.e., we measure time in days. In this case, the hour angle is $h = 2\pi t$ and the solar longitude is $\lambda = 2\pi t/365$. This fully specifies the insolation $S(t)$ at each latitude ϕ.

Next, we separate the insolation into discrete frequency components. For each latitude, we numerically generate a one-year time series of $S(t)$ at N evenly-spaced times. The mean value is

$$S_0 = \frac{1}{N}\Sigma S(t) \tag{4}$$

and we calculate each sinusoidal component n with period P_n using the Fourier transform,

$$Y_n = \frac{2}{N}\Sigma e^{2\pi i t/P_n} S(t), \tag{5}$$

where the factor of 2 accounts for both positive and negative frequencies. The amplitude (S_n) and phase (θ_n) of each Fourier component is given by

$$S_n = |Y|,\ \theta_n = \tan^{-1}\left[\frac{\mathrm{Im}(Y)}{\mathrm{Re}(Y)}\right]. \tag{6}$$

We isolate the annual ($P_1 = 365$), semiannual ($P_2 = 365/2$), and diurnal ($P_3 = 1$) components as the dominant frequencies of variability. Neglecting all other frequencies, the insolation is hence approximated as

$$S(t) \approx S_0 + S_1\cos\left(\frac{2\pi}{P_1}t - \theta_1\right) + S_2\cos\left(\frac{2\pi}{P_2}t - \theta_2\right) + S_3\cos\left(\frac{2\pi}{P_3}t - \theta_3\right). \tag{7}$$

In Fig. 8a,c, we plot the range of each frequency of net solar forcing, $2(1-\alpha_p)S_n$, as a function of latitude, where α_p is the planetary albedo. Diurnal variability dominates in low to mid latitudes and annual variability dominates in high latitudes. The semiannual component is important near the equator, where the sun passes overhead twice per year, as well as in high latitudes where polar night causes the seasonal variability to depart substantially from an annual sinusoid. The annual cycle dominates over the semiannual cycle in the latitudes of interest for this study (7°–14°), and this dominance is felt even more strongly at depth in the sandy regolith due to longer period variability penetrating more deeply (as described below). Hence for simplicity we focus here only on the annual and diurnal components of variability in solar radiation, S_1 and S_3.

Surface temperature

We let the annual and diurnal frequency components of the surface temperature evolution, T_n, evolve as a linear function of the net solar forcing, $(1-\alpha_p)S_n$. The proportionality constant is chosen based on modern observations of surface temperature variability over land. The physical basis for this relationship is discussed below.

We consider the evolution of the surface temperature (T_s) subject to solar insolation of a single frequency superimposed on the annual mean. Assuming a single column with no horizontal energy transport in the atmosphere, the surface temperature evolution can be approximated as

$$c_n \frac{dT_s}{dt} = (1-\alpha_p)\left[S_0 + S_n \cos\left(\frac{2\pi}{P_n}t - \theta_n\right)\right] - \left[L_m + L_T\left(T_s - T_m\right)\right]. \tag{8}$$

Here c_n is the heat capacity associated with changes in T_s on the timescale indicated by n. Since we are interested in the temperature variability at an ice-free location, we use an approximation of the ice-free modern planetary albedo based on satellite observations (Graves et al., 1993), $\alpha_p = 0.2 + 0.36\sin^2(\phi)$. The parameters L_m and L_T represent the infrared radiation to space as a linear function of the surface temperature, with T_m being the melting point; this approximation is commonly made in simple climate models (e.g., North et al., 1981). The linear system (8) can be solved exactly as

$$T_s = T_m + \frac{(1-\alpha_p)S_0 - L_m}{L_T} + T_n \cos\left(\frac{2\pi}{P_n}t - \tilde{\theta}_n\right) \tag{9}$$

with phase

$$\tilde{\theta}_n = \theta_n + \tan^{-1}\frac{2\pi c_n}{P_n L_T} \tag{10}$$

and amplitude

$$T_n \equiv \frac{(1-\alpha_p)S_n}{\sqrt{L_T^2 + (2\pi c_n/P_n)^2}}. \tag{11}$$

Here we have neglected the transient term in the solution to eq. (8) associated with the decay of the initial condition. Annual and diurnal amplitudes (T_n) can be considered together in this framework by linear superposition of the solutions for the two frequencies.

In principle, the entire denominator in eq. (11) is adjusted to match temperature variability over land in modern observations. This is equivalent to the more physically intuitive approach of letting $L_T = 2$ Wm^{-2}K^{-1}, which is a typical value used in simple climate models (e.g., North et al., 1981), and adjusting the parameter c_n which includes the heat capacity of the sandy regolith and the atmospheric column above. Due to the dependence of the diffusive penetration depth on the frequency of the forcing (as described in the following section), the diurnal cycle is not expected to have the same effective heat capacity as the annual cycle. Using the latter approach, we choose values of c_n for the diurnal and annual cycles to match the amplitudes of variability over land in modern observations (New et al., 1999) when the solar constant in the model is set to the modern value ($S_0 = 1370$Wm^{-2}), which leads to $c_1 = 3\times10^7$Jm^{-2}K^{-1} for the annual cycle and $c_3 = 0.1\times10^7$Jm^{-2}K^{-1} for the diurnal cycle. This set of parameters fully specifies the amplitudes of diurnal and annual cycles in surface temperature, T_n, which will be used in the following section to force variability within the regolith below. In Fig. 8b,d we plot the surface temperature annual range ($2T_1$) and diurnal range ($2T_3$) as a function of latitude.

We note that the planetary albedo above ice-free columns may likely have been different during a snowball glaciation compared with today due to differences in clouds and atmospheric composition. Similarly, the heat capacity of the atmospheric column may have been reduced due to the lower humidity. However, the dramatic differences in penetration depth between annual and diurnal forcing (Fig. 8) is expected to dominate over these factors.

Thermal diffusion in sandy regolith

We consider the ground as a one-dimensional thermally diffusive medium of infinite depth with sinusoidally-varying surface temperature specified from eq. (9)-(11). An alternative approach would have been to use a single thermodynamic model of the column of ground below an atmospheric column, but we choose to model the atmosphere–surface system separately (discussed above) as a forcing on the subsurface ground in order to more transparently match the surface temperature variability with modern observations. In the interior ($0 \leq z < \infty$), we model the temperature field $T(z,t)$ to evolve according to

$$\frac{\partial T}{\partial t} = \kappa \frac{\partial^2 T}{\partial z^2}, \tag{12}$$

with the surface boundary condition

$$T(0,t) = T_n \cos\left(\frac{2\pi}{P_n} t - \tilde{\theta}_n\right) \tag{13}$$

using T_n from eq. (11). A solution to this system is

$$T(z,t) = T_n e^{-z/\lambda} \cos\left(\frac{2\pi}{P_n} t - \tilde{\theta}_n - \frac{z}{\lambda}\right) \tag{14}$$

with

$$\lambda \equiv \sqrt{\frac{2\kappa P_n}{2\pi}}. \tag{15}$$

Note that here, as above, the response to the total forcing can be calculated using linear superposition of the separate frequencies. Using a sandy regolith thermal diffusivity of $\kappa = 1.1 \times 10^{-6}$ m^2/s as in previous work (Maloof et al., 2002), this leads to $\lambda = 0.17$m for diurnal variability and $\lambda = 3.3$m for annual variability. These values are shown with one significant figure in the main text. Note that thermal diffusivity values for sandstone are approximately the same as those used here, being $\kappa \approx 1.12 \times 10^{-6}$ m^2/s.

Heat transport into permafrost is typically modeled as a diffusive process (Riseborough et al., 2008). However, once melting occurs at the surface, advection of heat by liquid water (Rowland et al., 2011) could make our estimates of seasonal ground temperature fluctuations at depth conservative. Heat is also lost by the ground due to latent heating during the melt of the pore ice and gained during the freeze of the pore water, which would reduce our diffusive estimates of seasonal ground temperature fluctuations at depth by a factor that depends on the concentration of ice in the regolith. Note that these processes may also influence the value of c_n in eq. (11). The presence of sand wedges rather than ice wedges, as well as the aeolian sand sheet, suggests an arid paleoenvironment where ground ice concentrations, guided by modern observations (Berg and Black, 1966; Bockheim et al., 2007; Campbell et al., 1998), may have been only a few percent.

In order to get an approximate scaling for the influence of latent heat of phase changes within the regolith, we consider a phase boundary between liquid and solid that migrates vertically in a thermally diffusive medium in response to a change in the surface temperature, which is a Stefan problem. When the surface temperature above a frozen column of pure material is suddenly warmed to a temperature ΔT above the melting point, the liquid-solid interface will propagate downward according to

$$h = \sqrt{\frac{2\kappa c_p \Delta T t}{L}}, \tag{16}$$

where h is the depth of the interface, c_p is the specific heat capacity above the solid-liquid interface, L is the latent heat of fusion, and t is time (Worster, 2000). The solution (16) requires the approximation that the Stefan number, $S \equiv L/(c_p \Delta T)$, is large. Here we use the Stefan solution (16) to estimate the depth of thaw penetration, which is a standard procedure in permafrost modeling (Riseborough et al., 2008). We use a latent heat of fusion of $L = \gamma L_0$, where $L_0 = 3 \times 10^2$ J/g is the value for pure ice and γ is the fraction of the ground that is ice rather than sand. We use $c_p = 1$ J/g/K for the heat capacity of the sand/water mixture above the phase interface, which is a typical value for sand. We consider several values for the seasonal ground surface positive degree days, ΔTt. For a 14° paleolatitude with annual-mean temperature of 0°C, $\Delta Tt = T_1(1\text{yr})/\pi = 2.4$K yr, where $T_1 = 7.5$K is the surface temperature annual cycle amplitude (half the annual range plotted in Fig. 8b) and we have used that $\int_0^{0.5} \sin 2\pi x dx = 1/\pi$. Solving eq. (16) for γ, we find that in order for the thaw to penetrate to a depth of at least $h = 4m$ with these parameter values, the ice content of the regolith would have to be less than $\gamma = 0.03$. For a 14° paleolatitude with annual-mean temperature of 2.5°C, integration of the positive values of the vertically-shifted sinusoidal surface ground temperature yields $\Delta Tt = 1.3$K yr, which corresponds to an ice content of $\gamma = 0.02$ for 4m thaw penetration. For a 7° paleolatitude with annual-mean temperature of 0°C, $\Delta Tt = T_1(1\text{yr})/\pi = 1.2$K yr using $T_1 = 3.9$K from Fig. 8b, and $\gamma = 0.02$ for 4m thaw penetration. This implies that if only diffusion causes heat transport into the ground, the ice content of the regolith would have to be a few percent or less in order to allow periodic melting from the surface down to 4m depth driven by the seasonal surface temperature variations we calculate for 7° to 14° paleolatitude, with lower required ice contents for annual-mean temperatures farther from 0°C. Advection by liquid water, however, would allow for the possibility of larger ice contents within the ∼4m freeze-thaw zone.

References

Berg, T., Black, R., 1966. Preliminary measurements of growth of nonsorted polygons, Victoria Land, Antarctica. Antarctic Research Series, 61–108.

Bockheim, J. G., Campbell, I. B., McLeod, M., 2007. Permafrost distribution and active-layer depths in the McMurdo dry valleys, antarctica. Permafrost Periglacial Processes 18 (3), 217–227.

Campbell, I., Claridgei, G., Campbell, D., Balks, M., 1998. Permafrost properties in the McMurdo Sound-Dry Valley region of Antarctica. Permafrost – Seventh International Conference Proceedings, 121–126.

Graves, C. E., Lee, W. H., North, G. R., mar 20 1993. New parameterizations and sensitivities for simple climate models. Journal of Geophysical Research-Atmospheres 98 (D3), 5025–5036.

Hartmann, D. L., 1994. Global Physical Climatology. Academic Press.

Maloof, A. C., Kellogg, J. B., Anders, A. M., 2002. Neoproterozoic sand wedges: crack formation in frozen soils under diurnal forcing during a snowball earth. Earth and Planetary Science Letters 204 (1-2), 1–15.

New, M., Hulme, M., Jones, P., 1999. Representing twentieth-century space-time climate variability. Part I: development of a 1961-90 mean monthly terrestrial climatology. Journal of Climate 12 (3), 829–856.

North, G. R., Cahalan, R. F., Coakley, J. A., 1981. Energy balance climate models. Reviews of Geophysics and Space Physics 19, 91–121.

Pierrehumbert, R. T., 2011. Principles of Planetary Climate. Cambridge University Press.

Pierrehumbert, R. T., Abbot, D. S., Voigt, A., Koll, D., 2011. Climate of the neoproterozoic. Annual Review of Earth and Planetary Sciences 39, 417–460.

Riseborough, D., Shiklomanov, N., Etzelmuller, B., Gruber, S., Marchenko, S., 2008. Recent advances in permafrost modelling. Permafrost Periglacial Processes 19 (2), 137–156.

Rowland, J. C., Travis, B. J., Wilson, C. J., 2011. The role of advective heat transport in talik development beneath lakes and ponds in discontinuous permafrost. Geophysical Research Letters 38, L17504.

Worster, M., 2000. Solidification of fluids. In: Perspectives in Fluid Dynamics. Cambridge University Press, pp. 393–446.